Direct Control of Bearingless Permanent Magnet Synchronous Motor Based on Prediction Model

Huangqiu Zhu and Mingcan Wu[*]

Abstract—The direct control for the bearingless permanent magnet synchronous motor (BPMSM) has problems of large ripples of flux linkage, torque, and suspension force due to sampling time delay. To solve above problems, a predictive direct control method is proposed based on the traditional direct control by adding prediction model. Firstly, the generation principle of radial suspension forces of the BPMSM is introduced. Secondly, the models of the predictive direct control method are given based on the traditional direct control, and the time-delay compensation model is deduced. Thirdly, the predictive direct control system is constructed, and the simulations are carried out. Finally, the proposed control strategy is applied to a prototype, and the related experimental results are given and analyzed. The results of the simulations and experiments show that compared with the traditional direct control of the BPMSM, the predictive direct control strategy can effectively reduce the ripples of flux linkage, torque, and suspension forces, and improve the static and dynamic performance of the BPMSM.

1. INTRODUCTION

The traditional magnetic bearing has the advantages of no lubrication, no mechanical wear, low noise, and long service life. Bearingless permanent magnet synchronous motor (BPMSM) inherits the characteristics of magnetic bearing and the excellent operation characteristics of a permanent magnet synchronous motor, which has been paid more attention [1, 2]. Owing to low loss and high efficiency, BPMSM has been applied to aerospace, biomedicine, semiconductor manufacturing [3, 4], etc.

The control technology of the BPMSM has made great progress with the development of control technology in ordinary motor. The direct torque control (DTC) in an ordinary motor is a high performance variable frequency speed regulation method developed after the vector control technology [5]. The DTC based on space vector pulse width modulation (SVPWM) is applied to the BPMSM to realize direct torque control and direct suspension force control [6]. However, a traditional direct control system has many problems, such as not constant switching frequency of the inverter and sampling time delay, which is easy to cause the losses and ripples of flux linkage, torque, and suspension force. To overcome the problems, various methods have been proposed in the last few years, such as artificial intelligence techniques [7], fixed switching frequency techniques, and improving the controller techniques [8, 9]. The DTC based on space vector modulation is proposed in [10]. The switching frequency of this method is constant, which reduces the ripples of flux linkage and torque of motor and switching losses effectively, but the problem of sampling time delay is neglected.

With the same aim of reducing ripples and losses, predictive direct control has been gaining more attention. In all available predictive direct control strategies, predictive current control and predictive torque control are two most popular control methods [11–13]. Model predictive direct control has been widely applied to permanent magnet synchronous motors [14–17]. The electromagnetic torque and flux

linkage are predicted respectively by establishing the discretization model of the control system. The minimum optimal voltage vector is selected after the cost function is calculated. The high complexity of control strategy makes the main disadvantage.

In this paper, based on direct torque control and direct suspension control of the BPMSM, a predictive algorithm is proposed to predict the torque, flux linkage, and suspension forces of the next sampling period. The required voltage vector is synthesized based on SVPWM to realize the direct control of the BPMSM. The effectiveness of the control strategy is verified by simulations. Finally, the experiment is carried out on a BPMSM prototype, which has better dynamic and static performance. Compared with the traditional direct control method, the proposed control strategy reduces the ripples of flux linkage, torque, and suspension forces, which improve the stability and anti-interference ability of the BPMSM.

2. GENERATION PRINCIPLE OF RADIAL SUSPENSION FORCE

There are two sets of windings wound in the stator of the BPMSM, which are used to produce torque and suspension force. The windings that produce torque are called torque windings, whose pole-pair number is P_M, which is equal to the pole-pair number of rotor magnetic field. Another set of windings that produce suspension force together with torque windings is called suspension force windings, whose pole-pair number is P_B. In addition to producing torque, the torque windings also provide a bias magnetic field for the suspension force generation.

In the paper, $P_M = 1$ and $P_B = 2$ are adopted as pole-pair numbers of two sets of windings in the BPMSM, respectively. Because the pole-pair numbers of torque windings and suspension windings are different, the pole-pair numbers of the produced air-gap magnetic field are also different. The radial suspension force is produced by the unbalanced air-gap magnetic field. Figure 1 shows the principle of the radial suspension force of the BPMSM in the x- and y-directions. The flux linkage ψ_M is produced by torque windings and permanent magnet when the torque windings are excited. The flux linkage ψ_B is produced by suspension force windings when the suspension force windings are excited. Figure 1(a) shows that when the rotor is in the balanced position, two kinds of flux linkage with the same polarity are in the x positive direction, and two kinds of flux linkage with different polarities are in the x negative direction, which leads to the uneven magnetic field density of the left and right air gaps, resulting in the radial suspension force F_x in the x positive direction. When the suspension flux linkage is opposite with that in Figure 1(a), the radial suspension force in the x negative direction is produced. Similarly, the generation principle of radial suspension force in the y direction is showed in Figure 1(b).
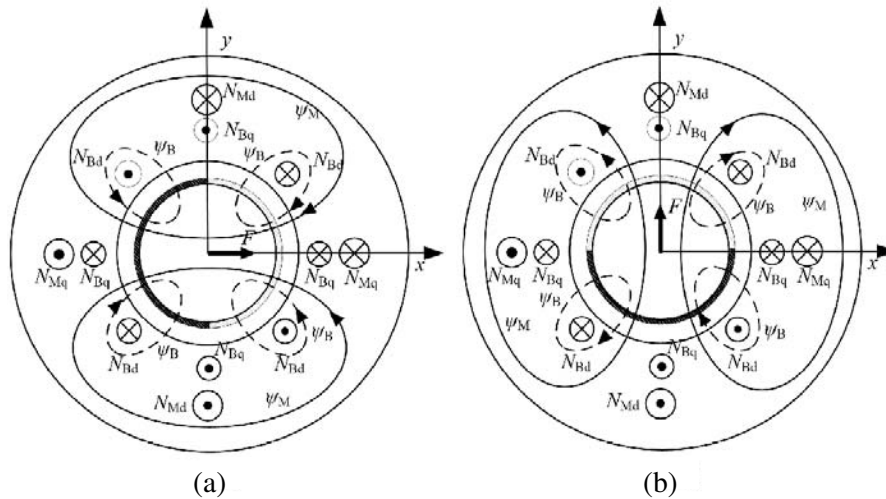
Figure 1. Generation principle of radial suspension force. (a) Suspension force in the x direction. (b) Suspension force in the y direction.

3. PREDICTIVE CONTROL MODEL OF BPMSM

3.1. Predictive Direct Torque Control of BPMSM

In the DTC method, the flux linkages of torque windings in the α- and β-axes are observed according to the current values and the flux linkage values of the permanent magnet. Then the feedback value of the torque is obtained by the relationship among the electromagnetic torque, flux linkage, and torque windings current in the two-phase static coordinate system. The error between the feedback value and the given value is modulated by PI controller to obtain the increment of the phase angle of the flux linkage of torque windings. The reference voltage calculated by the voltage vector calculation module is used as the input of SVPWM to realize the direct torque control of BPMSM.

According to the theory of the permanent magnet motor, the equations of voltage and flux linkages of the torque windings of the BPMSM in two-phase static coordinate system are obtained as [18]:

$$\begin{cases} u_{\mathrm{M}\alpha} = R_{\mathrm{M}} i_{\mathrm{M}\alpha} + \dfrac{\mathrm{d}\psi_{\mathrm{M}\alpha}}{\mathrm{d}t} \\[2mm] u_{\mathrm{M}\beta} = R_{\mathrm{M}} i_{\mathrm{M}\beta} + \dfrac{\mathrm{d}\psi_{\mathrm{M}\beta}}{\mathrm{d}t} \end{cases} \tag{1}$$

$$\begin{cases} \psi_{\mathrm{M}\alpha} = L_{\mathrm{s}} i_{\mathrm{M}\alpha} + \psi_{\mathrm{f}} \cos\theta \\ \psi_{\mathrm{M}\beta} = L_{\mathrm{s}} i_{\mathrm{M}\beta} + \psi_{\mathrm{f}} \sin\theta \end{cases} \tag{2}$$

where $u_{\mathrm{M}\alpha}$ and $u_{\mathrm{M}\beta}$ are equivalent torque winding voltages in α- and β-axes, respectively; $i_{\mathrm{M}\alpha}$ and $i_{\mathrm{M}\beta}$ are equivalent torque winding currents in α- and β-axes, respectively; $\psi_{\mathrm{M}\alpha}$ and $\psi_{\mathrm{M}\beta}$ are equivalent torque winding flux linkages in α- and β-axes, respectively; R_{M} is the resistance of torque windings; ψ_{f} is the flux linkage of the permanent magnet; L_{s} is the inductance of torque windings; θ is the rotor mechanical angle.

The electromagnetic torque equation can be obtained as [19]:

$$T_{\mathrm{e}} = \frac{3}{2} P_{\mathrm{M}} (\psi_{\mathrm{M}\alpha} i_{\mathrm{M}\beta} - \psi_{\mathrm{M}\beta} i_{\mathrm{M}\alpha}) \tag{3}$$

In the prediction algorithm of direct torque control, there are two steps. The first step is to observe flux linkage based on the current value of the sampling point (assumed as time k) by Equation (2). The second step is to predict the flux linkage and current at the next time (time $k + 1$) and calculate the predicted torque.

To predict the value at next step, the forward Euler discretization equation is considered as:

$$\frac{\mathrm{d}x}{\mathrm{d}t} \approx \frac{x(k+1) - x(k)}{T_{\mathrm{s}}} \tag{4}$$

where T_{s} is the sampling time of the system.

Assuming that the current time is k, the prediction expression of stator flux linkage at time $k + 1$ according to Equation (1) is obtained as follows:

$$\begin{cases} \psi_{\mathrm{M}\alpha}(k+1) = \psi_{\mathrm{M}\alpha}(k) + [u_{\mathrm{M}\alpha}(k) - R_{\mathrm{M}} i_{\mathrm{M}\alpha}(k)] T_{\mathrm{s}} \\ \psi_{\mathrm{M}\beta}(k+1) = \psi_{\mathrm{M}\beta}(k) + [u_{\mathrm{M}\beta}(k) - R_{\mathrm{M}} i_{\mathrm{M}\beta}(k)] T_{\mathrm{s}} \end{cases} \tag{5}$$

Then using the current component in d-q coordinate system to predict the current component of the next step, the current component of torque windings of BPMSM in d-q coordinate system is obtained as:

$$\begin{cases} i_{\mathrm{Md}} = \displaystyle\int \frac{u_{\mathrm{Md}} - R_{\mathrm{M}} i_{\mathrm{Md}} + \omega L_{\mathrm{Md}} i_{\mathrm{Md}}}{L_{\mathrm{Md}}} \mathrm{d}t \\[3mm] i_{\mathrm{Mq}} = \displaystyle\int \frac{u_{\mathrm{Mq}} - R_{\mathrm{M}} i_{\mathrm{Mq}} - \psi_{\mathrm{f}} - \omega L_{\mathrm{Mq}} i_{\mathrm{Mq}}}{L_{\mathrm{Mq}}} \mathrm{d}t \end{cases} \tag{6}$$

where ω is the electric angular frequency; L_{Md} and L_{Mq} are the equivalent inductances of torque windings in d- and q-axes, respectively; u_{Md} and u_{Mq} are equivalent torque winding voltages in d- and q-axes, respectively; i_{Md} and i_{Mq} are equivalent torque winding currents in d- and q-axes, respectively.

From Equation (6), the current prediction expression in d-q coordinate system can be obtained as:

$$\begin{cases} i_{\mathrm{Md}}(k+1) = i_{\mathrm{Md}}(k) + \dfrac{u_{\mathrm{Md}}(k) - R_{\mathrm{M}}i_{\mathrm{Md}}(k) + \omega L_{Md}i_{\mathrm{Md}}(k)}{L_{Md}}T_{\mathrm{s}} \\ i_{\mathrm{Mq}}(k+1) = i_{\mathrm{Mq}}(k) + \dfrac{u_{\mathrm{Mq}}(k) - R_{\mathrm{M}}i_{\mathrm{Mq}}(k) - \psi_{\mathrm{f}} - \omega L_{\mathrm{Mq}}i_{\mathrm{Mq}}(k)}{L_{\mathrm{Mq}}}T_{\mathrm{s}} \end{cases} \tag{7}$$

$i_{\mathrm{M}\alpha}(k+1)$ and $i_{\mathrm{M}\beta}(k+1)$ can be obtained by the park inverse transformation of $i_{\mathrm{Md}}(k+1)$ and $i_{\mathrm{Mq}}(k+1)$. According to Equations (3), (5), and (7), the predictive expression of torque can be obtained as:

$$T_{\mathrm{e}}(k+1) = \frac{3}{2}P_{\mathrm{M}}[\psi_{\mathrm{M}\alpha}(k+1)i_{\mathrm{M}\beta}(k+1) - \psi_{\mathrm{M}\beta}(k+1)i_{\mathrm{M}\alpha}(k+1)] \tag{8}$$

3.2. Predictive Direct Suspension Force Control of BPMSM

Direct suspension force control includes the closed loop control of suspension force and the closed loop control of rotor radial displacement. In a two-phase static coordinate system, the feedback value of suspension force is calculated according to the observed flux linkage of torque windings and the flux linkage of suspension force windings. Then according to the error between the given value and the feedback value of suspension force, the increment of the flux linkage of the suspension force windings is obtained. Through SVPWM and inverter, the direct suspension force control of BPMSM is realized. According to the principle of the BPMSM, Figure 2 is the flux linkage vector diagram of BPMSM.
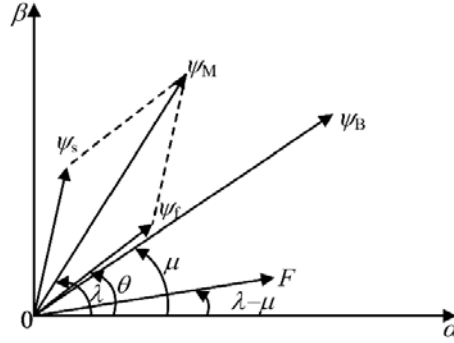
Figure 2. Flux linkage vector diagram of BPMSM.

The mathematical model of suspension force expressed by flux linkage is written as [6]:

$$\begin{cases} F_\alpha = k_{\mathrm{m}}\psi_{\mathrm{M}}\psi_{\mathrm{B}}\cos(\lambda - \mu) \\ F_\beta = k_{\mathrm{m}}\psi_{\mathrm{M}}\psi_{\mathrm{B}}\sin(\lambda - \mu) \end{cases} \tag{9}$$

where ψ_{M} and ψ_{B} are flux linkages of torque windings and suspension force windings, respectively; λ is the phase angle of flux linkage in torque windings, $\lambda = \arctan(\psi_{\mathrm{M}\alpha}/\psi_{\mathrm{M}\beta})$; μ is the phase angle of flux linkage in suspension force windings, $\mu = \arctan(\psi_{\mathrm{B}\alpha}/\psi_{\mathrm{B}\beta})$; k_{m} is the constant term, $k_{\mathrm{m}} = \pi P_{\mathrm{M}}P_{\mathrm{B}}/8lr\mu_0 N_1 N_2$; r is the radius of rotor; l is the length of the motor core; N_1 and N_2 are the turns of torque windings and suspension force windings, respectively; μ_0 is the air gap length.

The flux linkage of the suspension force windings is produced when the suspension force windings are excited. The equations of voltage of suspension force windings can be obtained as

$$\begin{cases} u_{\mathrm{B}\alpha} = R_{\mathrm{B}}i_{\mathrm{B}\alpha} + \dfrac{\mathrm{d}L_{\mathrm{B}}i_{\mathrm{B}\alpha}}{\mathrm{d}t} \\ u_{\mathrm{B}\beta} = R_{\mathrm{B}}i_{\mathrm{B}\beta} + \dfrac{dL_{\mathrm{B}}i_{\mathrm{B}\beta}}{\mathrm{d}t} \end{cases} \tag{10}$$

where L_{B} is the self-inductance of suspension force windings; $i_{\mathrm{B}\alpha}$ and $i_{\mathrm{B}\beta}$ are the equivalent suspension force winding currents in the α- and β-axes, respectively; R_{B} is the resistance of suspension force windings.

From Equation (9), the suspension force is determined by the flux linkages of torque windings and suspension force windings. It can be assumed that the position of the rotor remains unchanged in a very small period Δt. At this point, it can be approximately assumed that the amplitude of the rotor winding flux linkage ψ_M and phase λ are constant. The relationship between increment of suspension force and increment of flux linkage of suspension force windings can be expressed as:

$$\begin{pmatrix} \Delta F_\alpha \\ \Delta F_\beta \end{pmatrix} = k_m \psi_M \begin{pmatrix} \cos\lambda & \sin\lambda \\ \sin\lambda & -\cos\lambda \end{pmatrix} \begin{pmatrix} \Delta\psi_{B\alpha} \\ \Delta\psi_{B\beta} \end{pmatrix} \tag{11}$$

According to the increment of flux linkage, the reference voltage value is calculated as

$$\begin{cases} u_{B\alpha}^* = R_B i_{B\alpha} + \Delta\psi_{B\alpha} \\ u_{B\beta}^* = R_B i_{B\beta} + \Delta\psi_{B\beta} \end{cases} \tag{12}$$

The prediction of the suspension force is also divided into two steps. The first step is to observe the flux linkage of the suspension force windings and the torque windings according to the sampling current at time k. The observed value of the suspension force is obtained from Equation (9). The second step is to predict the flux linkage of torque windings according to Equation (5), and the flux linkage of suspension force windings is predicted by Equation (13). The prediction of the flux linkage of suspension force windings can be obtained as

$$\begin{cases} \psi_{B\alpha}(k+1) = \psi_{B\alpha}(k) + [u_{B\alpha}(k) - R_B i_{B\alpha}(k)] T_s \\ \psi_{B\beta}(k+1) = \psi_{B\beta}(k) + [u_{B\beta}(k) - R_B i_{B\beta}(k)] T_s \end{cases} \tag{13}$$

From Equation (9), the predicted value of suspension force at the next time can be obtained as

$$\begin{cases} F_\alpha(k+1) = k_m \psi_m(k+1)\psi_B(k+1)\cos(\lambda - \mu) \\ F_\beta(k+1) = k_m \psi_m(k+1)\psi_B(k+1)\sin(\lambda - \mu) \end{cases} \tag{14}$$

According to Equations (11) and (12), the voltage reference values of predictive direct suspension force control can be obtained as:

$$\begin{cases} u_{B\alpha}^* = R_B i_{B\alpha}(k+1) + k_m^{-1}\psi_M^{-1}(k+1)(\Delta F_\alpha \cos\lambda + \Delta F_\beta \sin\lambda) \\ u_{B\beta}^* = R_B i_{B\beta}(k+1) + k_m^{-1}\psi_M^{-1}(k+1)(\Delta F_\alpha \cos\lambda - \Delta F_\beta \sin\lambda) \end{cases} \tag{15}$$

4. TIME-DELAY COMPENSATION

In ideal simulation, the current and voltage measurements are taken at time k, and the accurate reference voltage is obtained at time k. However, the microprocessor needs time to execute the algorithm in a real experiment, and if the variables are measured at time k, a sampling period is required to generate the optimal switching state. Therefore, the selected voltage vector is given to the inverter at time $k + 1$ instead of time k. In order to compensate the delay time, the values of flux linkage, torque, and suspension force are predicted at time $k + 2$ on the basis of the original prediction of time $k + 1$. The most effective drive and the reference voltage vector at time $k + 1$ are obtained, which makes up for the time delay calculated by the algorithm and realizes the consistency of time.

The predicted flux linkages, currents, and torque of torque windings at time $k + 2$ are obtained as

$$\begin{cases} \psi_{M\alpha}(k+2) = \psi_{M\alpha}(k+1) + [u_{M\alpha}(k+1) - R_M i_{M\alpha}(k+1)]T_s \\ \psi_{M\beta}(k+2) = \psi_{M\beta}(k+1) + [u_{M\beta}(k+1) - R_M i_{M\beta}(k+1)]T_s \end{cases} \tag{16}$$

$$\begin{cases} i_{Md}(k+2) = i_{Md}(k+1) + \dfrac{u_{Md}(k+1) - R_M i_{Md}(k+1) + \omega L_{Md} i_{Md}(k+1)}{L_{Md}} T_s \\ i_{Mq}(k+2) = i_{Mq}(k+1) + \dfrac{u_{Mq}(k+1) - R_M i_{Mq}(k+1) - \psi_f - \omega L_{Md} i_{Md}(k+1)}{L_{Mq}} T_s \end{cases} \tag{17}$$

$$T_e(k+2) = \frac{3}{2}P_M[\psi_{M\alpha}(k+2)i_{M\beta}(k+2) - \psi_{M\beta}(k+2)i_{M\alpha}(k+2)] \tag{18}$$

The predicted flux linkage of suspension force windings and suspension force at time $k + 2$ are obtained as

$$\begin{cases} \psi_{\text{B}\alpha}(k + 2) = \psi_{\text{B}\alpha}(k + 1) + [u_{\text{B}\alpha}(k + 1) - R_{\text{B}}i_{\text{B}\alpha}(k + 1)]T_{\text{s}} \\ \psi_{\text{B}\beta}(k + 2) = \psi_{\text{B}\beta}(k + 1) + [u_{\text{B}\beta}(k + 1) - R_{\text{B}}i_{\text{B}\beta}(k + 1)]T_{\text{s}} \end{cases} \tag{19}$$

$$\begin{cases} F_\alpha(k + 2) = k_{\text{m}}\psi_{\text{M}}(k + 2)\psi_{\text{B}}(k + 2)\cos(\lambda - \mu) \\ F_\beta(k + 2) = k_{\text{m}}\psi_{\text{M}}(k + 2)\psi_{\text{B}}(k + 2)\sin(\lambda - \mu) \end{cases} \tag{20}$$

5. PREDICTIVE DIRECT CONTROL SYSTEM OF BPMSM

According to predictive direct torque and suspension force control algorithm, a predictive direct control system for BPMSM is constructed. The control block diagram is shown in Figure 3.
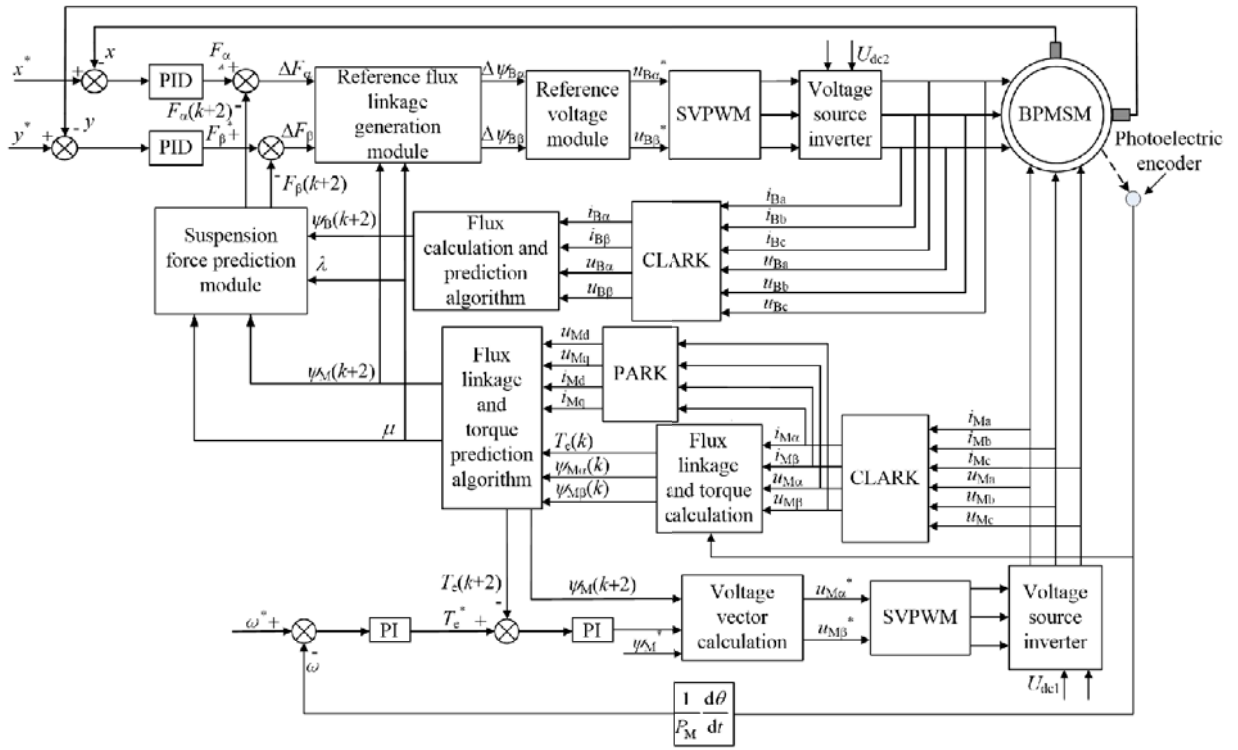
Figure 3. Predictive direct control diagram of BPMSM.

The control system can be divided into predictive direct torque subsystem and predictive direct suspension force subsystem. In the predictive direct torque subsystem, the rotor angle θ is detected by photoelectric encoder, which is used to calculate rotor speed ω. The error between the rotor speed and the given rotor speed ω^* is regulated by a PI controller to produce the given torque T_{e}^*. The given torque is compared with the torque $T_{\text{e}}(k + 2)$ in the prediction module. The torque error is regulated by the PI controller to produce the power angle increment. According to the given flux linkage ψ_{m}^* of the torque windings and the predicted flux linkage $\psi_{\text{M}}(k + 2)$ of torque windings in the prediction module, the reference voltages u_α^* and u_β^* are obtained. The switching signal of the inverter is given by SVPWM. The closed-loop operation of predictive direct torque control of BPMSM is realized.

In the predictive direct suspension force subsystem, the displacement x and y are detected by the displacement sensor. The error between the displacement and given displacement is regulated by the PID controller to produce the given suspension force F_α^* and F_β^*, which is compared with the suspension force in the prediction module. The increment of the flux linkage of suspension force windings is obtained

by the reference flux linkage generation module. The increment of the space voltage vector of the suspension force windings is obtained through the reference voltage module. The switching signal of the inverter is given through SVPWM, which is transported to the BPMSM to realize the double closed loop control of the direct suspension force of the BPMSM.

6. SIMULATION AND EXPERIMENT

6.1. Simulation Result Analysis

In order to verify the effectiveness of the proposed method, the simulations of the proposed method and traditional direct control method are performed in the MATLAB/Simulink environment. The starting time and termination time of the simulation are 0 s and 0.2 s, respectively. Simulation parameters are set as: the air gap is 1 mm; the initial position of rotor is $x = -0.25$ mm, $y = -0.35$ mm; the motor speed is set to 6000 r/min. Figure 4 shows the simulation waveforms of speed in two methods. In Figure 4, the speed response time of the proposed method is shorter than the traditional method; the speed is stable; the speed response is fast; and there is no overshoot basically, which shows the good speed regulation performance.
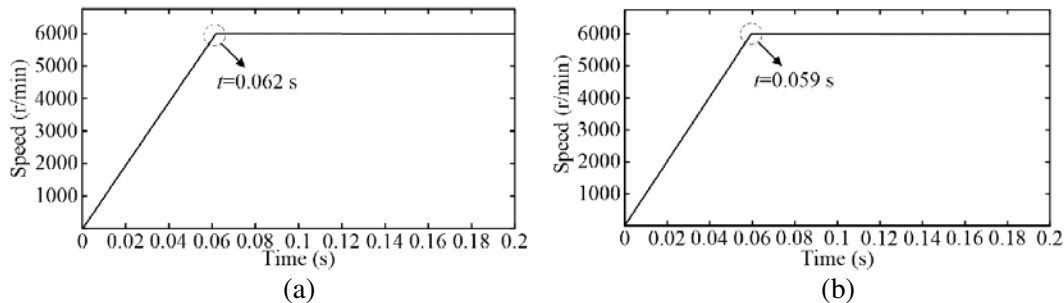
Figure 4. The simulation waveforms of speed in two methods. (a) Traditional direct control method. (b) Predictive direct control method.

The initial load torque is $1 \, \mathrm{N \cdot m}$, and the load torque is added to $3.5 \, \mathrm{N \cdot m}$ at 0.12 s. Then, the output torques of two methods are simulated. The simulation waveforms of torque are shown in Figure 5. The torque ripples of the traditional direct control are about $0.5 \, \mathrm{N \cdot m}$, and the torque ripples of predictive direct control are only about $0.2 \, \mathrm{N \cdot m}$. It can be concluded that the proposed method can significantly reduce the torque ripple. The simulation waveforms of flux linkage in two methods are shown in Figure 6. After using the proposed method, the flux linkage of torque windings in the BPMSM is obviously improved, and the flux linkage ripple is reduced.
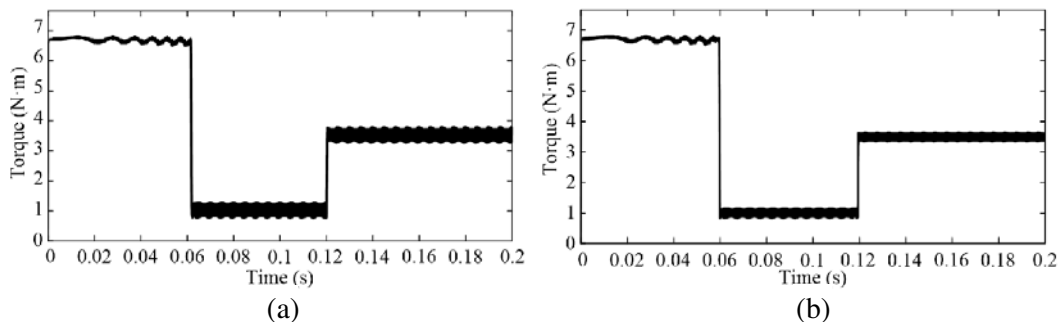
Figure 5. The simulation waveforms of torque in two methods. (a) Traditional direct control method. (b) Predictive direct control method.
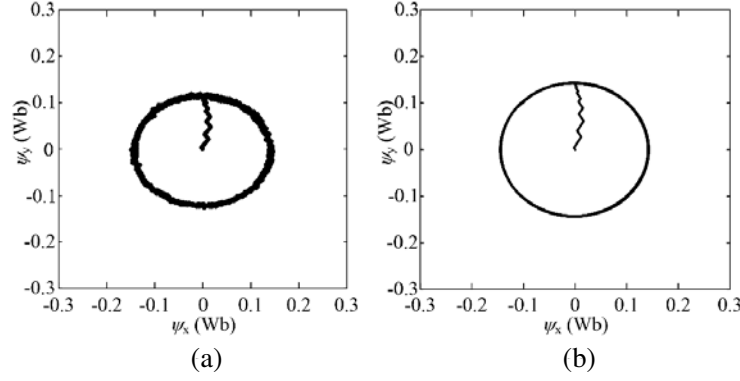
Figure 6. The simulation waveforms of flux linkage in two methods. (a) Traditional direct control method. (b) Predictive direct control method.
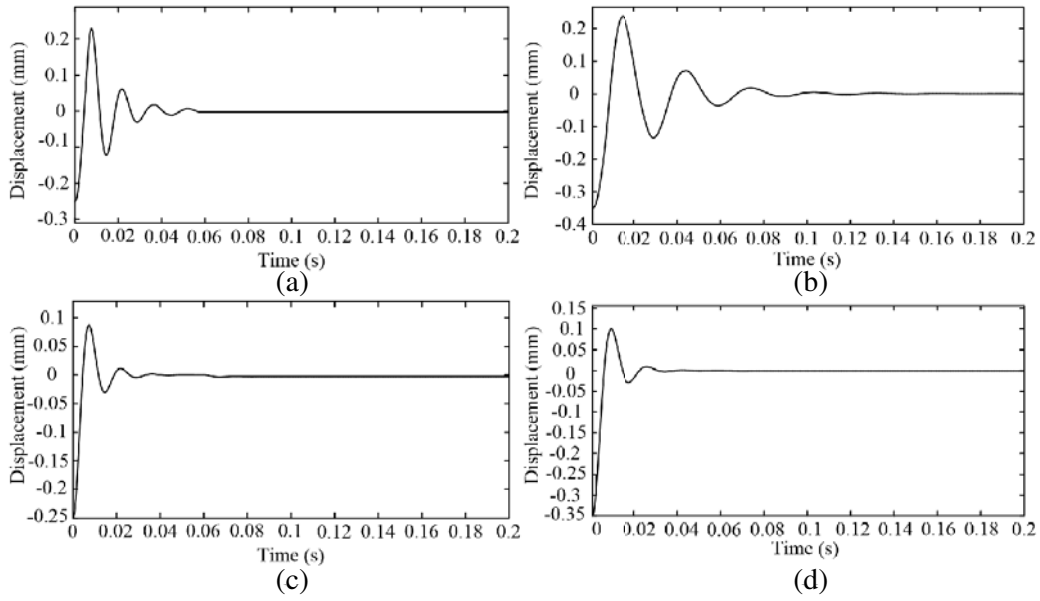
Figure 7. The simulation waveforms of radial displacement in two methods. (a) Displacement of traditional direct control method in the x direction. (b) Displacement of traditional direct control method in the y direction. (c) Displacement of predictive direct control method in the x direction. (d) Displacement of predictive direct control method in the y direction.

The simulation waveforms of radial displacement in two methods are shown in Figure 7. When the motor is set at the same offset position, the rotor can be recovered to the balanced position faster, and the fluctuation decreases with the predictive direct control system. In the traditional direct control system, the rotor is restored to the balanced position in the x direction after 0.06 s and in the y direction after 0.11 s, respectively. In predictive direct control system, the rotor is restored to the balanced position in the x direction after 0.03 s and in the y direction after 0.032 s, respectively. It shows that the proposed prediction direct control not only preserves the excellent operation characteristics of the traditional direct control algorithm, but also improves the performance of the motor.

6.2. Experiment Result Analysis

The predictive direct control algorithm proposed in this paper is applied to a BPMSM prototype. Figure 8 shows the experimental platform of the BPMSM. The parameters of the prototype are shown
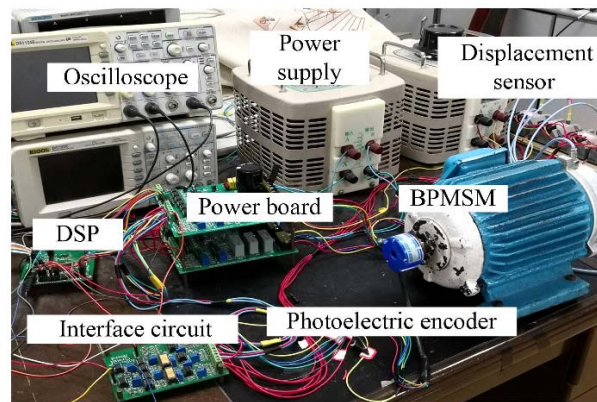
Figure 8. Experimental platform of BPMSM.

Table 1. Parameters of BPMSM.

Parameters	value
Rated power (kW)	1.1
Rated speed (r/min)	6000
Pole-pair number of torque windings	1
Pole-pair number of suspension force windings	2
Flux linkage of permanent magnet (Wb)	0.125
Permanent magnet material	NFeB35
Length of air gap (mm)	1
Length of rotor axial (mm)	20
Length of air gap (mm)	0.25
Rotor rotary inertia $(\text{kg} \cdot \text{m}^2)$	0.0056

in Table 1. The proposed control method is implemented by a digital signal processor (DSP) of TMS320F28335.

The experimental results are shown in Figure 9, Figure 10, and Figure 11. Figure 9 shows the radial displacement waveforms in two methods when the motor is running steadily. The speed is 1000 r/min. The displacement fluctuations of BPMSM are about 12 μm in the x- and y-directions when traditional direct control method is applied. When the proposed control method is applied to the motor, the displacement fluctuations are about 8 μm in the x- and y-directions. It can be seen that the control accuracy of the radial suspension force of the motor is improved by the proposed control algorithm in this paper, and the motor has better control performance.

Figure 10 shows the comparison of dynamic performance when the proposed control method and traditional control method are applied to the prototype, respectively. The given speed of the prototype rises from 1000 r/min to 2800 r/min. The predictive control algorithm takes 80 ms, and the speed ripples are 120 r/min while the traditional control algorithm takes 110 ms, and the speed ripples are 160 r/min. It can be seen that the speed response of the proposed control algorithm is faster, and the running of motor is more stable. In the process of speed rising, the displacement ripples increase. After the speed is stable, the motor continues to maintain steady suspension. The radial displacement in the x direction (similar to y direction) slightly increases, but the difference is very small, which indicates that the coupling relationship between the torque subsystem and suspension subsystem is very small, and the direct suspension force control used in the suspension subsystem has good dynamic performance.

Figure 11 shows a comparison of the radial displacement waveforms when the rotor is subjected
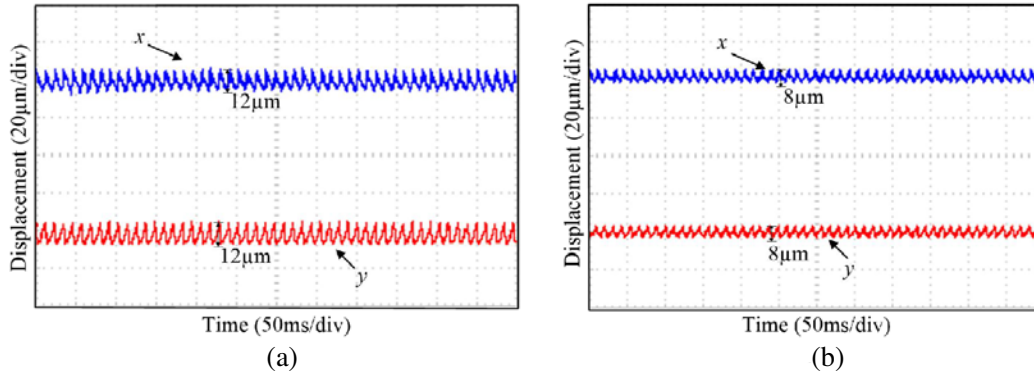
Figure 9. Radial displacement waveforms. (a) Traditional direct control method. (b) Predictive direct control method.
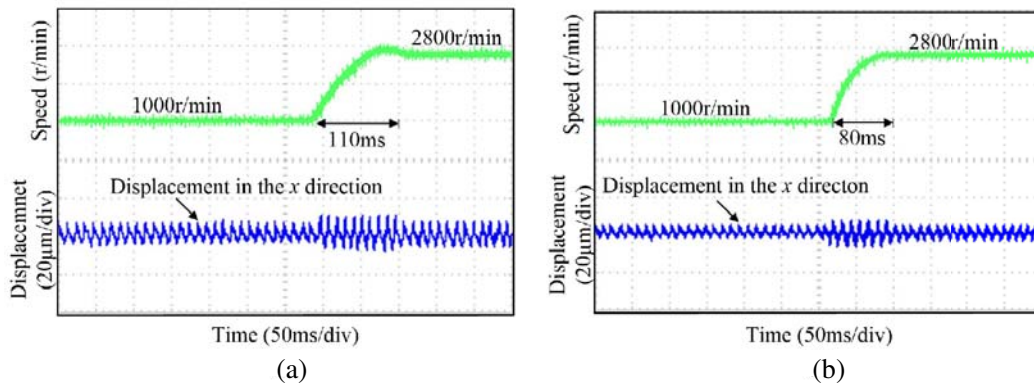
Figure 10. Experimental results of BPMSM speed regulation. (a) Traditional direct control method. (b) Predictive direct control method.
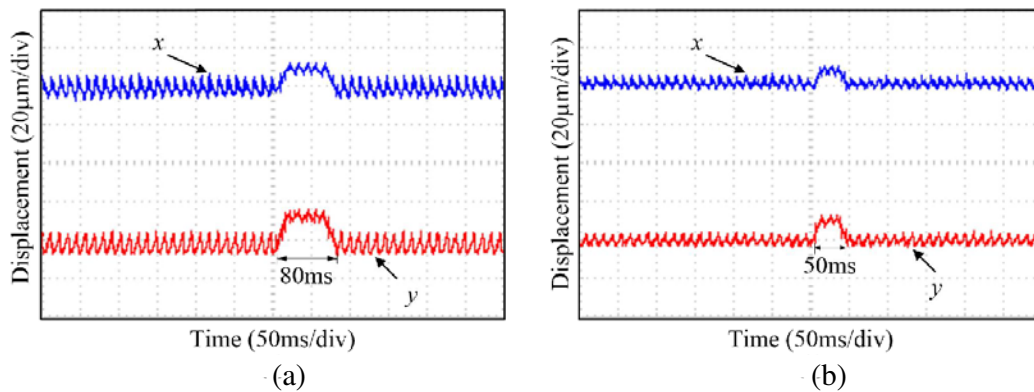
Figure 11. Radial displacement waveforms with external disturbance. (a) Traditional direct control method. (b) Predictive direct control method.

to external interference. When the motor is running at the speed of $1000\,\mathrm{r/min}$, the rotor suspends steadily in the balanced position and suddenly adds a radial interference force of $10\,\mathrm{N}$ in the y direction. It can be seen that the displacement error of the rotor in the y direction is more than that in the x direction. After a brief adjustment of the suspension force subsystem, the rotor can quickly return to the balanced position and continue to maintain a stable suspension. The radial displacement waveform

in the y direction can be seen in Figure 11, which shows that the recovery time of conventional direct control method is 80 ms, and that of proposed control method in this paper is 50 ms. Therefore, the control method proposed in this paper can improve the anti-interference ability of the motor.

7. CONCLUSION

In this paper, the predictive control algorithm is added to the traditional direct control, which makes up for the defect of the sampling time delay and improves the stability of the motor. The simulated and experimental results show that compared with the traditional direct control, the proposed predictive direct control reduces the ripples of flux linkage, torque, and suspension forces of the BPMSM. When the rotor is subjected to external disturbance, the BPMSM rotor can be suspended and operated stably. Therefore, the BPMSM with predictive direct control system has better dynamic and static performance and anti-interference ability.

ACKNOWLEDGMENT

REFERENCES

1. Zhu, H. and Z. Gu, "Active disturbance rejection control of 5-degree-of-freedom bearingless permanent magnet synchronous motor based on fuzzy neural network inverse system," *ISA Transactions*, Vol. 101, 295–308, Jun. 2020.

2. Zhao, C. and H. Zhu, "Design and analysis of a novel bearingless flux-switching permanent magnet motor," *IEEE Transactions on Industrial Electronics*, Vol. 64, No. 8, 6127–6136, Aug. 2017.

3. Sun, X., L. Chen, and Z. Yang, "Overview of bearingless permanent magnet synchronous motors," *IEEE Transactions on Industrial Electronics*, Vol. 60, No. 12, 5528–5538, Dec. 2013.

4. Zhang, S. and F. L. Luo, "Direct control of radial displacement for bearingless permanent-magnet-type synchronous motors," *IEEE Transactions on Industrial Electronics*, Vol. 56, No. 2, 542–552, Feb. 2009.

5. Takahashi, I. and T. Noguchi, "A new quick-response and high-efficiency control strategy of an induction motor," *IEEE Transactions on Industry Applications*, Vol. IA-22, No. 5, 820–827, Sept. 1986.

6. Zhu, H., et al., "Direct torque and direct suspension force control of bearingless permanent magnet synchronous motor," *Proc. Int. Conf. Chinese Control and Decision Conference (CCDC)*, 2411–2415, Xuzhou, 2010.

7. Naik, N. V., A. Panda, and S. P. Singh, "A three-level fuzzy-2 DTC of induction motor drive using SVPWM," *IEEE Transactions on Industrial Electronics*, Vol. 63, No. 3, 1467–1479, Mar. 2016.

8. Iacchetti, M. F., G. D. Marques, and R. Perini, "Torque ripple reduction in a DFIG-DC system by resonant current controllers," *IEEE Transactionson Power. Electronics*, Vol. 30, No. 8, 4244–4254, Aug. 2015.

9. Ammar, A., et al., "Predictive direct torque control with reduced ripples and fuzzy logic speed controller for induction motor drive," *Proc. Int. Conf. International Conference on Electrical Engineering-Boumerdes (ICEE-B)*, 1–6, Boumerdes, 2017.

10. Ammar, A., B. Abdelhamid, and B. Amor, "Closed loop torque SVM-DTC based on robust super twisting speed controller for induction motor drive with efficiency optimization," *International Journal of Hydrogen Energy*, Vol. 42, No. 28, 17940–17952, Apr. 2017.

11. Wang, F., et al., "Model-based predictive direct control strategies for electrical drives: An experimental evaluation of PTC and PCC methods," *IEEE Transactions on Industrial Informatics*, Vol. 11, No. 3, 671–681, Jun. 2015.

12. Correa, P., M. Pacas, and J. Rodriguez, "Predictive torque control for inverter-fed induction machines," *IEEE Transactions on Industrial Electronics*, Vol. 54, No. 2, 1073–1079, Apr. 2007.

13. Li, C., et al., "An improved finite-state predictive torque control for switched reluctance motor drive," *IET Electric Power Applications*, Vol. 12, No. 1, 144–151, Jan. 2018.

14. Xiao, M., et al, "Predictive torque control of permanent magnet synchronous motor using flux vector," *IEEE Transactions on Industry Applications*, Vol. 54, No. 5, 4437–4446, Sept.–Oct. 2018.

15. Cao, B., et al., "Direct torque model predictive control of a polyphase permanent magnet synchronous motor with current harmonic suppression and loss reduction," *Proc. Int. Conf. IEEE Applied Power Electronics Conference and Exposition (APEC)*, 2460–2464, San Antonio, 2018.

16. Hanke, S., O. Wallscheid, and J. Bocker, "A direct model predictive torque control approach to meet torque and loss objectives simultaneously in permanent magnet synchronous motor applications," *Proc. Int. Conf. Predictive Control of Electrical Drives and Power Electronics (PRECEDE)*, 101–106, Pilsen, 2017.

17. Wang, T., et al., "Model predictive torque control of permanent magnet synchronous motors with extended set of voltage space vectors," *IET Electric Power Applications*, Vol. 11, No. 8, 1376–1382, Sept, 2017.

18. Zhang W., et al., "Direct control of bearingless permanent magnet slice motor based on active disturbance rejection control," *IEEE Transactions on Applied Superconductivity*, Vol. 30, No. 4, 1–5, Jun. 2020.

19. Sun X., et al., "High-performance control for a bearingless permanent-magnet synchronous motor using neural network inverse scheme plus internal model controllers," *IEEE Transactions on Industrial Electronics*, Vol. 63, No. 6, 3479–3488, Jun. 2016.